An Analytical Investigation of Swirl in Annular Propulsive Nozzles

Barbara T. Kornblum,* H. Doyle Thompson,† and Joe D. Hoffman‡
Purdue University, West Lafayette, Indiana

An analytical performance prediction methodology for annular propulsive nozzles with swirl introduced in the combustor upstream of the nozzle is presented. The application of that methodology to a specific nozzle design for a free vortex swirl distribution is discussed. Discharge coefficients, specific impulses, and wall pressure distributions are presented. These numerical studies show that the discharge coefficient, thrust, and specific impulse decrease as the amount of swirl increases. This methodology will enable nozzle designers to account for the effects of swirl in nozzle design.

Nomenclature

a = speed of sound
C_1-C_4 = constants specifying tangential velocity distributions
F = thrust
$\dot{m}$ = mass flow rate
M = Mach number
P, P_0 = static and stagnation pressure, respectively
R = gas constant
S = swirl number
t = time
T, T_0 = static and stagnation temperature, respectively
u, v, w = velocity components
x, y = axial and radial coordinates, respectively
yw = swirl
Y_1, Y_2 = inner and outer radii of the nozzle
γ = specific heat ratio
θ = tangential coordinate
ρ = density

Subscripts

A...F = geometric stations
IVL = initial-valve line
B, C, P = base, cowl, and plug, respectively
t, x, y = partial differentiation

Introduction

RECENT studies indicate that the introduction of swirl ahead of the combustor in axisymmetric dump combustors can have very beneficial effects on the combustion process. Buckley et al.[1] found that swirl both reduced the reattachment length of the combustor flowfield (thereby reducing the overall combustor length needed for good performance), and helped eliminate destructive very-low-frequency instabilities. They further concluded that (in the range of swirl intensities of their study), "losses in thrust due to residual swirl, at least to the sonic point of the nozzle, are negligible."

Scharrer and Lilley[2] made five-hole pitot probe measurements of the effects of swirl in simulated dump combustors followed by a nozzle. They observed a significant interaction between the swirling flowfield in the simulated combustor and the nozzle flowfield. Their major objective, however, was the measurement of the confined turbulent flow in the simulated combustor, not the nozzle flowfield. Consequently, their nozzles simply were used as downstream blockage components. Both nozzles used in their studies were conventional converging nozzles without centerbodies.

Conley et al.[3] presented an analytical and experimental investigation of the performance of annular propulsive nozzles without swirl. The present work is an extension of the performance prediction methodology developed by Conley et al. to include the effects of swirl introduced in the combustor on the performance of annular propulsive nozzles.

A similar study, performed by Dutton,[4] shows trends similar to the results obtained in the present investigation for conventional convergent-divergent nozzles without centerbodies. The present investigation is concerned with convergent-divergent nozzles with centerbodies.

The objective of the present work is to analytically investigate the effect of swirl on the transonic and supersonic flowfields in annular propulsive nozzles, and to determine the effects of swirl on mass flow rate, thrust, and specific impulse.

Performance Prediction Methodology

Geometric Model

The geometric model considered in this investigation is illustrated in Fig. 1. Air enters at station A and flows through a swirler where tangential momentum is transferred to the air to give the desired tangential velocity distribution at station B. Station B is followed by a sudden expansion dump into the combustor inlet at station C. Combustion takes place between stations C and D, where the stagnation temperature T_0 rises corresponding to the amount of fuel added and the stagnation pressure P_0 decreases slightly due to friction, mixing, and heat addition. The combustion products accelerate in the nozzle to the choked condition at the nozzle throat, station E, after which the flow continues to accelerate supersonically from station E to F.

The concern in the present study was the effect of swirl induced in the swirler on the performance of the nozzle (i.e., mass flow rate, thrust, and specific impulse). Consequently, the swirler, sudden expansion dump, and combustor are not modeled in detail in the present analysis. Emphasis is placed on the nozzle flowfield. However, the swirler is the source of the swirl in the flowfield. In the present analysis, the swirl

Presented as Paper 85-0364 at the AIAA 23rd Aerospace Sciences Meeting, Reno, NV, Jan. 14-17, 1985; received March 12, 1985; revision received July 12, 1985.

*Graduate Student; presently, Mechanical Engineer, Nuclear Test Division, Lawrence Livermore National Laboratory, Livermore, CA. Member AIAA.

†Professor of Mechanical Engineering, Thermal Sciences and Propulsion Center. Associate Fellow AIAA.

‡Professor of Mechanical Engineering, Thermal Sciences and Propulsion Center. Member AIAA.

introduced by the swirler is assumed to flow through the combustor and nozzle unchanged in magnitude.

Swirler

The swirler is a set of axial-flow guide vanes that imparts the desired tangential velocity distribution to the air as it passes through the swirler. The design of the swirler and the interaction of the swirl with the combustion process are of paramount importance in an actual system design. In the present study of the effects of swirl on nozzle performance, a tangential velocity distribution representative of that produced by a swirler and combustor is simply assumed to exist at the nozzle inlet, station D in Fig. 1.

Buckley et al.[1], by means of experiments, investigated four types of tangential velocity distributions at the swirler exit. They are:

$$\text{Constant angle:} \quad w = C_1 \; u = u \tan\alpha \tag{1}$$

$$\text{Forced vortex:} \quad w = C_2 y \tag{2}$$

$$\text{Free vortex:} \quad w = C_3/y \tag{3}$$

$$\text{Rankine vortex} \quad w = (C_4/y)[1 - \exp(-y^2/Y_2^2)] \tag{4}$$

where the constants C_1 to C_4 are specified to achieve the desired tangential velocity distribution. The only tangential velocity distribution considered in the present study was the free vortex distribution specified by Eq. (3). The free vortex distribution was selected because it is the only distribution that maintains itself at all axial locations. For example, a constant-angle swirl distribution at the swirler exit, station B, will produce an entirely different distribution at the nozzle entrance, station D. A centerbody exists throughout the flowfield, therefore, the singularity associated with the core of a free vortex does not occur in this flowfield.

In order to provide a basis for comparison of different swirlers, a swirl number S is employed, which is defined as

$$S = \int_{Y_1}^{Y_2} uwy^2 \mathrm{d}y \Big/ Y_2 \int_{Y_1}^{Y_2} u^2 y \mathrm{d}y \tag{5}$$

For a free vortex, $yw = C_3$, so that at a uniform flow section where the radial velocity $v = 0$ and the axial velocity u is uniform, Eq. (5) simplifies to

$$S = C_3/uY_2 \tag{6}$$

Consequently, the swirl number S is a simple function of the geometry (i.e., Y_2) and the axial velocity u. For choked flow, the average (one-dimensional) axial velocity u_D at the nozzle inlet can be estimated from the nozzle area ratio. Thus, for a given value of C_3, the swirl number S_D can be calculated. The corresponding values of swirl number at the combustor inlet S_C, swirler exit S_B, and nozzle throat S_E, can be estimated from the known value of S_D for a specified flow geometry and stagnation temperature rise in the combustor.

The major process occurring between stations C and D is the increase in stagnation temperature T_0 due to combustion. For a Rayleigh line flow (i.e., stagnation temperature change at constant area) in the absence of swirl, u_C can be calculated, so that

$$\frac{S_D}{S_C} = \frac{C_3/u_D Y_{2D}}{C_3/u_C Y_{2D}} = \frac{u_C}{u_D} \tag{7}$$

At the sudden expansion dump location, Y_2 changes from Y_{2B} to Y_{2C}. For constant mass flow rate $\dot{m}$, neglecting the centerbody area and compressibility effects which are both small, u is inversely proportional to the flow area, which is directly proportional to Y_2^2. Thus,

$$\frac{S_C}{S_B} = \frac{C_3/u_C Y_{2C}}{C_3/u_B Y_{2B}} = \frac{Y_{2C}}{Y_{2B}} \tag{8}$$

At the nozzle throat, station E, u_E is 3-5 times as large as u_D, and Y_{2E} may be 50-90% of Y_{2D}. When specific values are known, S_E can be calculated from S_D.

Consequently, for a specified value of the swirl yw at the nozzle inlet, the swirl number S_D at the nozzle inlet can be calculated. Knowing the other motor operating parameters, the values of the swirl number S can be estimated at other locations in the motor.

Performance Model

Figure 2 illustrates the thrust-producing components of a generic annular nozzle. The nozzle thrust is composed of the thrust developed 1) across the initial-value line F_{IVL}, 2) by the pressure acting on the cowl F_C, 3) by the pressure acting on the plug F_P, and 4) by the pressure acting on the plug base F_B. Thus the pressure distributions along the cowl and plug and the base pressure must be calculated to enable the calculation of the nozzle performance.

Flowfield Model

The accuracy and efficiency of nozzle performance prediction techniques are highly dependent on the flowfield model chosen to represent the actual flowfield. In the present study, the flowfield model is based on the following assumptions: 1) steady axisymmetric flow, 2) inviscid nonconducting fluid, 3) no body forces, 4) thermally and calorically perfect gas, and 5) empirical separation and base pressures.

The governing equations consist of the continuity equation, the component momentum equations, the energy equation, and the thermal and caloric equations of state. A detailed discussion of these equations is presented in Ref. 5.

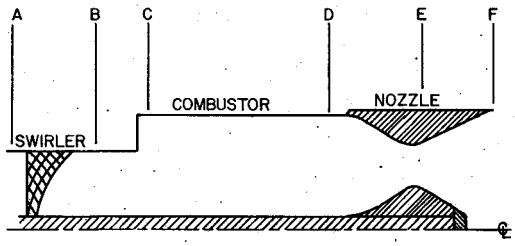

Fig. 1 Geometric model.

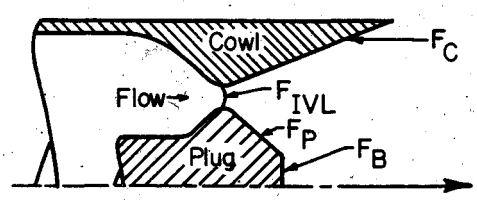

Fig. 2 Thrust-producing components of an annular nozzle.

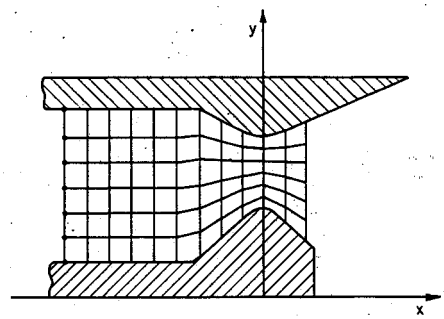

Fig. 3 Typical SNAP grid.

The choice of a numerical method, or methods, to solve these governing equations is also crucial to the success of the performance prediction procedure. A subsonic/transonic solution is required to define the mass flow rate and throat thrust, while a supersonic solution is required to define the nozzle, centerbody, and base thrusts. Experience[3] has shown that subsonic/transonic flowfields can be adequately determined from the steady-state solution to time-marching finite difference solutions, whereas the method of characteristics is the most accurate means for determining supersonic flowfields in nozzles. That is the approach taken in the present investigation.

Subsonic/Transonic Flowfield

The finite difference code developed to solve the subsonic/transonic flowfield is a modification of the VNAP (Viscous Nozzle Analysis Program) code developed by Cline[6] to include the effects of swirl. The resulting code is called SNAP (Swirling Nozzle Analysis Program).

The VNAP code was used as the subsonic/transonic flowfield prediction code for the annular nozzle performance prediction methodology developed by Conley et al.[3] The VNAP code solves the Navier-Stokes equations for two-dimensional (planar or axisymmetric), time-dependent, compressible flow using the second-order accurate, MacCormack finite difference scheme.[7] Inviscid flowfields can be solved by setting all of the viscous terms to zero, which yields the Euler equations. In the present study, the VNAP code was used as an inviscid flowfield solver. Explicit artificial diffusion is included in the code for shockwave calculations. However, no artificial diffusion was required in the present study, because only the subsonic/transonic portion of the flowfield was analyzed with the VNAP code. The steady-state solution is obtained as the asymptotic solution for large time.

The computational grid employed by the VNAP code is a transformed equally spaced grid. Equally spaced lines of constant ζ normal to the x axis comprise one of the transformed coordinates. Each vertical line segment between the plug and the cowl is divided into a number of equally spaced increments. Lines of constant η join these points. The physical grid is illustrated in Fig. 3. The transformation equations are

$$\zeta = x \quad \text{and} \quad \eta = \frac{y - Y_1(x)}{Y_2(x) - Y_1(x)} \tag{9}$$

where $Y_1(x)$ is the plug contour and $Y_2(x)$ the cowl contour.

In the present investigation, the VNAP code was modified to account for the presence of swirl in the flowfield by adding the tangential momentum equation to the set of governing equations, and the term $\rho w^2/y$ to the radial momentum equation. Since the flowfield is axisymmetric, all derivatives with respect to the tangential direction θ are zero, even though the tangential velocity component w is nonzero. The governing equations for this flowfield are

$$\rho_t + u\rho_x + v\rho_y + \rho u_x + \rho v_y + \rho v/y = 0 \tag{10}$$

$$\rho u_t + \rho u u_x + \rho v u_y + P_x = 0 \tag{11}$$

$$\rho v_t + \rho u v_x + \rho v v_y + P_y - \rho w^2/y = 0 \tag{12}$$

$$w_t + u w_x + v w_y + v w/y = 0 \tag{13}$$

$$P_t + u P_x + v P_y - a^2(\rho_t + u\rho_x + v\rho_y) = 0 \tag{14}$$

For a perfect gas,

$$P = \rho R T \quad \text{and} \quad a^2 = \gamma P/\rho \tag{15}$$

Equation (13) can be written as

$$\frac{D(yw)}{Dt} = 0 \tag{16}$$

which is in substantial derivative form. Equation (16) states that the swirl yw remains constant on the pathlines (i.e., paths traced by discrete fluid particles) of an unsteady flowfield and on the streamlines (i.e., lines everywhere tangent to the velocity vector) of a steady flowfield. Consequently, if the distribution of the swirl yw is specified in the upstream flowfield (specifically at the swirler exit, station B), that swirl distribution will be preserved throughout the nozzle flowfield.

The initial tangential velocity distribution $w(y)$ is specified at station B, an upstream station at the exit of the swirler. The mass flow rate distribution $\dot{m}(y)$ is computed at station B, so that the swirl yw is a known function of $\dot{m}$. This function, $yw(\dot{m})$, is then used to compute the swirl yw at each point in the nozzle in the following manner. After each time step, the mass flow rate is integrated across the flowfield at each axial location, from the centerbody ($\dot{m}=0$) to the nozzle wall ($\dot{m}=\dot{m}_{\text{tot}}$). The fractional mass flow rate at each radial position is calculated by dividing the calculated mass flow rate at that radial position by the total mass flow rate at that axial location. The resulting fractional mass flow rate is then used to interpolate for the swirl yw at the corresponding computational grid point by quadratic interpolation of the swirl function $yw(\dot{m})$ computed at station B. The swirl velocity w is then computed by dividing the interpolated value of the swirl yw by the value of y at the computational grid point.

This procedure is consistent with the governing partial differential equations only at the steady-flow limit, because actual unsteady pathlines are not tracked. Essentially, this procedure matches a normalized steady mass flow rate at the swirler exit to a normalized mass flow rate at each point in the nozzle. In an unsteady flow, these two points would not necessarily lie on the same pathline. However, at the steady-flow limit, these two points do lie on the same streamline, since pathlines and streamlines coincide in a steady flow.

In a typical run, 800-1000 time steps are taken by the SNAP code to relax the initially assumed one-dimensional flowfield to a steady state. An initial-value line along which the projection of the Mach number in the xy plane is supersonic is then specified across the throat region. This line was specified as a circular arc passing through the minimum radius point on the upper wall, the maximum radius point on the centerbody, and a point located radially midway between the two wall points and far enough downstream so that the projected Mach number is greater than 1.0 at all points on the circular arc. Values of the projected Mach number, flow angle, and tangential velocity along that line are determined by interpolation of the SNAP flowfield. Least squares quadratic bivariate interpolating polynomials are fit to the nine closest SNAP grid points to each initial-value line point. In this manner, a supersonic initial-value line is determined that can be used to initiate the solution of the supersonic flowfield by the method of characteristics.

Supersonic Flowfield

The supersonic flowfield is calculated by the method of characteristics for steady two-dimensional flow. For steady flow, Eqs. (10-15) apply with the time derivatives set to zero. The derivation of the corresponding characteristic and compatibility equations is a straightforward, although somewhat lengthy procedure. The derivation is presented by Kornblum and Thompson.[8] The results are not presented here. In brief, three characteristics are determined in the xy plane: the streamline and the right- and left-running Mach lines. Three compatibility equations are determined along the streamline and one compatibility equation is determined along each Mach line. These five compatibility equations are used to solve

for u, v, w, P, and ρ. The method is general so that any consistent initial swirl distribution can be treated.

A direct-marching method of characteristics procedure is employed to solve the characteristic and compatibility equations. The solution procedure constructs the Mach line network illustrated in Fig. 4. The characteristic and compatibility equations are integrated numerically by the second-order accurate modified-Euler predictor-corrector method. The solution is initiated from the supersonic initial-value line, line TT′, determined from the SNAP analysis. The projected Mach number (in the xy plane) along the space-like initial-value line must be supersonic. Left-running Mach lines are emanated from line TT′, starting at point T, and continued across the flowfield until they intersect the cowl, contour TE. The last such Mach line from point T′ intersects the cowl at point T″. Left-running Mach lines are then originated from points on the centerbody and continued across the flowfield to intersect the nozzle wall. This procedure is continued until the nozzle exit lip point E is determined. Left-running Mach lines are then terminated at the last right-running Mach line emanating from point E. This procedure is continued until point F at the end of the plug is determined. When Mach lines of the same family coalesce, embedded shock waves are formed. In the computer program, when Mach lines coalesce one of the Mach lines is discontinued. This procedure works well for weak shock waves.

The base pressure on the face of the truncated plug is computed from the empirical correlation proposed by Johnson[9]:

$$P_{\text{base}} = 0.846\, P_F / M_F^{1.3} \tag{17}$$

It should be noted that Eq. (17) only fits measured data when the base area is small. It gives unrealistically high values for highly truncated plugs and expansion-deflection nozzles.

The preceding procedure determines all of the data required to evaluate the thrust components illustrated in Fig. 2.

Results

Nozzle flowfields were computed for the 12 cases defined in Table 1. Figure 5 defines the flowfield geometry for all 12 cases. Only free vortex swirlers were considered. For free vortex swirlers, the swirl yw is constant everywhere in the flowfield. Thus, the tangential velocity component w can be computed at any location in the nozzle at any time step, independent of the streamline tracking procedure described previously. However, the general procedure was employed in the calculations presented in this section. The free vortex swirl distribution was chosen in this study to test the concept, and because free vortex swirlers are an important class of swirlers.

The swirl strength was characterized by the selected values of the swirl yw. Values of the swirl yw of 0, 50, 100, 150, 200, and 250 ft^2/s were analyzed for stagnation temperatures of 2500 and 3500 °R at the nozzle inlet. The stagnation pressure was 35 psia in every case. In all cases, the specific heat ratio $\gamma = 1.40$ and the gas constant $R = 53.35$ (ft-lbf)/(1bm-°R).

The swirl number S, defined by Eq. (5), varies with axial location in the flowfield. Table 1 gives approximate values of S at stations B, C, D, and E corresponding to the selected values of swirl yw, for the specific geometry presented in Fig. 5. The stagnation temperature at stations B and C was assumed to be 1000 °R.

Figure 6 presents constant Mach number lines in the transonic region for case 7 ($T_0 = 3500$ °R, $yw = 0$) as computed by the SNAP code. Comparisons with the constant Mach number lines for the other 11 cases show differences in the third significant figure for most quantities. Thus, Fig. 6 is representative of the plots for all 12 cases. There are some differences, however, which are discernible in the intergrated mass flow rate values tabulated in Table 2.

Figures 7 and 8 present the left-running Mach line pattern in the xy plane for the supersonic flowfields for cases 1 (no swirl) and 6 ($yw = 250$ ft^2/s). The left-running Mach lines emanating from the plug surface in these figures are terminated at the right-running Mach line emanating from the end of the cowl. Comparison of Figs. 7 and 8 shows that the Mach lines are steeper for the flowfield with swirl. This is due in part to the fact that the Mach lines are based on the projected Mach number for the swirling flow.

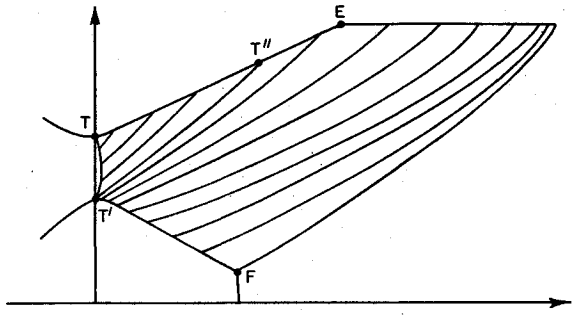

Fig. 4 Typical left-running Mach lines for supersonic annular swirling flow.

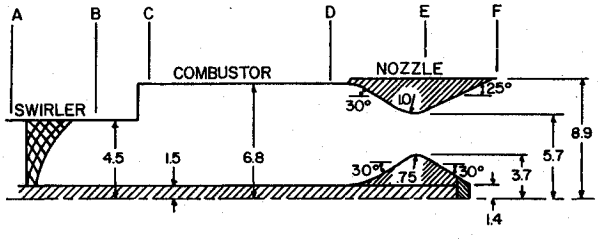

Fig. 5 Nozzle geometric specification.

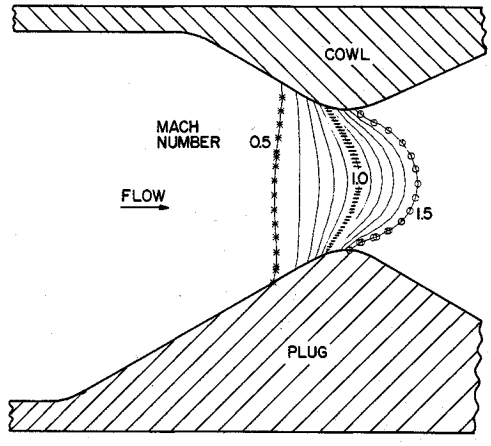

Fig. 6 Transonic Mach number distribution for case 7.

Table 1 Scope of the parametric study

Case No.	Swirl yw, ft^2/s	T_0, °R	Approximate swirl numbers			
			S_B	S_C	S_D	S_E
1	0	2500	0.00	0.00	0.00	0.000
2	50	2500	0.24	0.36	0.14	0.047
3	100	2500	0.48	0.73	0.28	0.094
4	150	2500	0.72	1.09	0.42	0.141
5	200	2500	0.96	1.45	0.56	0.188
6	250	2500	1.20	1.82	0.71	0.235
7	0	3500	0.00	0.00	0.00	0.000
8	50	3500	0.29	0.43	0.12	0.039
9	100	3500	0.57	0.86	0.24	0.079
10	150	3500	0.86	1.30	0.36	0.118
11	200	3500	1.14	1.73	0.48	0.158
12	250	3500	1.43	2.16	0.60	0.197

Figure 9 is a comparison of the static pressure distributions on the plug for cases 1 and 6. There is a substantial pressure decrease on the plug due to the effects of swirl. The pressure distributions for the intermediate values of swirl lie between the results of cases 1 and 6 in a very orderly fashion.

Figure 10 presents the pressure distributions on the cowl for cases 1 and 6. The pressure distributions on the cowl surface are almost indistinguishable for all swirl values. However, there are some differences in the integrated thrust values tabulated in Table 3. Because the projected cowl area is large, a small pressure difference produces distinguishable differences in the integrated thrust values.

Table 2 summarizes the mass flow rates, discharge coefficients, and specific impulses for the 12 cases studied. The reference (one-dimensional) mass flow rate is 21.984 lbm/s for cases 1 to 6, and 18.580 lbm/s for cases 7 to 12. Mass flow rates were determined by integrating across the initial-value line obtained from the SNAP analysis. The zero swirl discharge coefficient (0.9776) reflects the two-dimensional nature of the flowfield and is a function of the transonic geometry. The discharge coefficients are plotted in Fig. 11. The values decrease with increasing swirl in a smooth, consistent manner and indicate consistency in the initial-value data obtained from the SNAP analysis. Figure 12 is a plot of the vacuum specific impulses as a function of swirl. The figure illustrates that there is a real loss of performance due to the effects of swirl, and that the loss is nonlinear, becoming much more severe as the swirl increases.

The individual thrust contributions from the initial-value line, cowl, plug, and base (illustrated in Fig. 2) are tabulated in Table 3. The thrust values are computed from the method of characteristics analysis and all values are referenced to zero ambient pressure.

For case 3 $yw = 100$ ft^2/s), the swirl number at station B is 0.48, which is representative of a typical situation. For that value of swirl, the effect of swirl, as ascertained from Table 3, is not very significant. The mass flow rate is reduced by about 0.66% (see Table 2), the thrust across the initial-value line is decreased by 0.77%, and the overall thrust is reduced by about 0.82%. The thrust reduction due to pressure forces on the cowl is very small, but the reduction in thrust on the plug is more significant. The effect of swirl is to produce a positive radial pressure gradient so that the cowl pressures are increased and the plug pressures are decreased due to the swirl alone.

For the higher values of swirl (case 6, $yw = 250$ ft^2/s), the decreases in thrust are larger in all categories. The effects are nonlinear, so that increasing the swirl from $yw = 200$ to 250 ft^2/s has a much greater effect than increasing from $yw = 0$ to 50 ft^2/s.

The following observations for free vortex swirlers in annular nozzles can be made from the results obtained in this study.

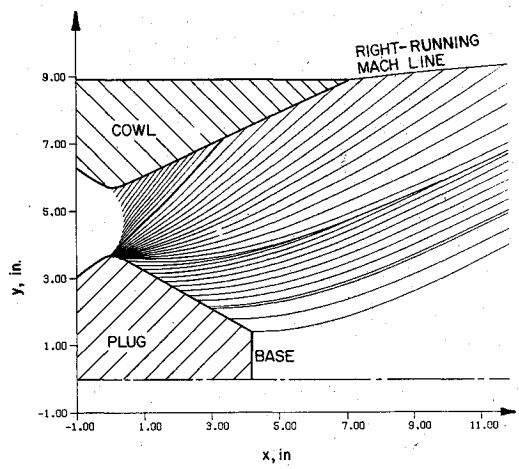

Fig. 7 Left-running Mach lines for case 1.

1) The data are extremely consistent, giving a high degree of confidence in the trends. The thrust values for cases 1 and 7 are essentially identical. This is, of course, what one would hope, since changing the stagnation temperature does not affect the absolute thrust values. However, the initial-value line calculated by the SNAP code might be expected to be somewhat different, since the flow speeds and permissible time steps for those calculations are different. This result gives confidence in the consistency of the results.

2) For those applications for which $yw < 100$ ft^2/s, the effect of swirl on the mass flow rate, thrust values, and specific

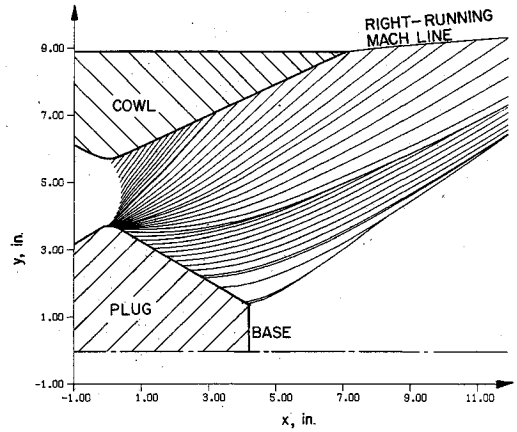

Fig. 8 Left-running Mach lines for case 6.

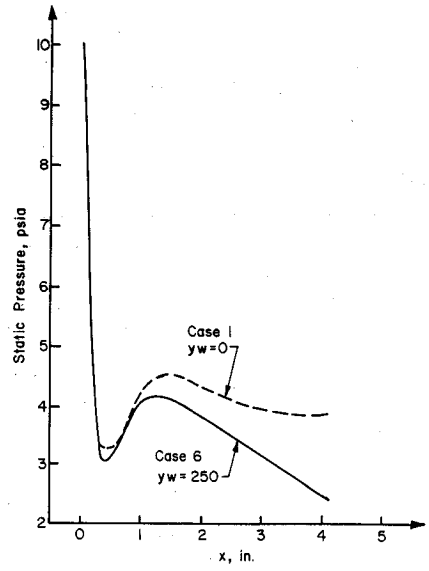

Fig. 9 Pressure distributions on the plug for cases 1 and 6.

Table 2 Comparison of mass flow rate and specific impulse

Case No.	Swirl yw, ft^2/s	T_0, °R	Mass flow, lbm/s	C_D	I_{sp}, lbf-s/lbm
1	0	2500	21.491	0.9776	141.614
2	50	2500	21.456	0.9760	141.555
3	100	2500	21.350	0.9712	141.385
4	150	2500	21.173	0.9631	141.115
5	200	2500	20.929	0.9520	140.728
6	250	2500	20.611	0.9375	140.255
7	0	3500	18.163	0.9776	167.562
8	50	3500	18.142	0.9764	167.511
9	100	3500	18.078	0.9730	167.367
10	150	3500	17.971	0.9672	167.135
11	200	3500	17.823	0.9593	166.806
12	250	3500	17.633	0.9490	166.399

Table 3 Comparison of thrust values

Case No.	Thrust, lbf				
	F_{IVL}	Cowl	Plug	Base	Total
1	2582.08	298.25	155.34	7.76	3043.43
2	2577.11	298.01	154.44	7.64	3037.20
3	2562.23	297.30	151.75	7.30	3018.58
4	2537.58	296.10	147.38	6.76	2987.82
5	2503.38	294.40	141.47	6.04	2945.29
6	2459.43	291.70	134.49	5.18	2890.80
7	2582.08	298.25	155.34	7.76	3043.43
8	2578.53	298.08	154.70	7.68	3038.99
9	2567.89	297.57	152.77	7.43	3025.66
10	2550.23	296.71	149.61	7.04	3003.59
11	2525.67	295.51	145.30	6.51	2972.99
12	2494.37	293.94	139.94	5.86	2934.11

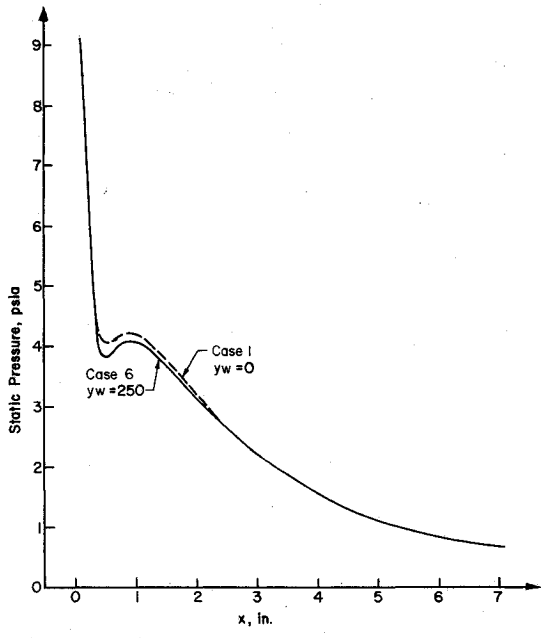

Fig. 10 Pressure distributions on the cowl for cases 1 and 6.

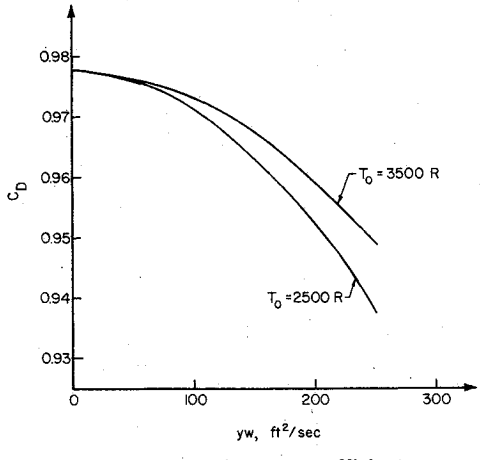

Fig. 11 Discharge coefficients.

impulse is small and probably can be ignored in preliminary design and overall performance considerations.

3) At higher values of swirl, the overall thrust is degraded significantly by the effects of swirl. In some cases, a part of the thrust degradation can be compensated for in the design by increasing the throat area to compensate for the decreased mass flow rate. When geometric constraints restrict the nozzle exit area, such a design change may not produce the desired overall result. In any case, there is a real loss in specific impulse for high swirl flows that cannot be recovered.

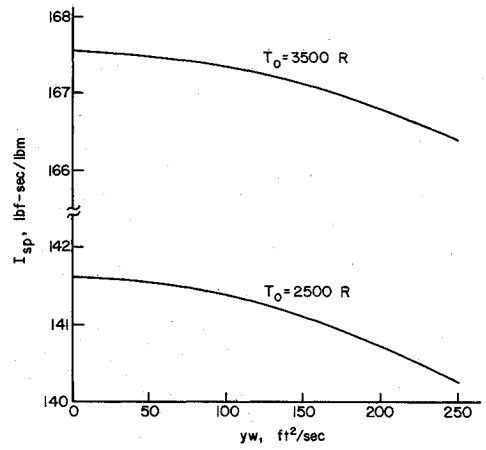

Fig. 12 Vacuum specific impulses.

4) When the cowl and plug surfaces are contoured to optimize the nozzle performance as, for example, in Ref. 9, the optimum contour will be affected by the presence of swirl in the flowfield.

Conclusions

An analytical performance prediction methodology for analyzing the effects of swirl in annular propulsive nozzles has been developed. Computed results for a series of swirl intensities for free vortex swirlers are extremely consistent and indicate a high degree of reliability in the results. The presence of swirl decreases the discharge coefficient, thrust, and vacuum specific impulse of a nozzle. For values of swirl often encountered in ramjet and turbojet applications, the effect of swirl on the nozzle performance is small, and probably can be neglected in preliminary design and performance calculations. Experimental verification of the results is needed. Application of the methodology to other than free vortex swirlers is needed.

Acknowledgments

This work was sponsored by the Aero Propulsion Laboratory, Air Force Wright-Aeronautical Laboratories, Wright-Patterson Air Force Base, OH. Mr. John R. Smith was the Air Force Project Engineer.

References

[1]Buckley, P. L., Craig, R. R., Davis, D. L., and Schwartzkopf, K. G., "The Design and Combustion Performance of Practical Swirlers for Integral Rocket/Ramjets," *AIAA Journal*, Vol. 21, May 1983, pp. 733-740.

[2]Scharrer, G. L. and Lilley, D. G., "Five-Hole Pitot Probe Measurements of Swirl, Confinement and Nozzle Effects on Confined Turbulent Flow," AIAA Paper 84-1605, June 1984.

[3]Conley, R. R., Hoffman, J. D., and Thompson, H. D., "An Analytical and Experimental Investigation of Annular Propulsive Nozzles," *Journal of Aircraft*, Vol. 22, April 1985, pp. 270-276.

[4]Dutton, J. C., "Time-Dependent Calculations of Swirling Nozzle Flow," 1983 USAF-SCEEE Summer Faculty Research Program, Air Force Office of Scientific Research, Final Report, Aug. 1983.

[5]Zucrow, M. J. and Hoffman, J. D., *Gas Dynamics*, Vol. 1, John Wiley and Sons, New York, 1975, Chap. 10.

[6]Cline, M. C., "VNAP: A Computer Program for Computation of Two-Dimensional, Time-Dependent, Viscous, Internal Flow," Los Alamos Scientific Laboratory, Los Alamos, NM, Rept. LA-7326, Nov. 1978.

[7]MacCormack, R. W., "The Effect of Viscosity in Hypervelocity Impact Cratering," AIAA Paper 69-354, April 1969.

[8]Kornblum, B. T. and Thompson, H. D., "A Method of Characteristics Program for Computing Annular Nozzle Flowfields with Swirl," Thermal Sciences and Propulsion Center, Purdue University, West Lafayette, IN, Rept. ME-TSPC-84-01, July 1984.

[9]Johnson, G. R., "Design of Maximum Thrust Plug Nozzles with Variable Inlet Geometry," Ph.D. Thesis, Purdue University, West Lafayette, IN, Jan. 1972.